A Sensorless Direct Torque Control Scheme Suitable for Electric Vehicles

Farid Khoucha, Khoudir Marouani, Abdelaziz Kheloui, Mohamed Benbouzid

A Sensorless Direct Torque Control Scheme Suitable for Electric Vehicles

Farid Khoucha, Khoudir Marouani, Abdelaziz Kheloui and Mohamed El Hachemi Benbouzid

***Abstract*—In this paper a sensorless control is proposed to increase the efficiency of a Direct Torque Control (DTC) of an induction motor propelling an Electric Vehicle (EV). The proposed scheme uses an adaptive flux and speed observer that is based on a full order model of the induction motor. Moreover, it is evaluated on an EV global model taking into account the vehicle dynamics. Simulations were first carried out on a test vehicle propelled by a 37-kW induction motor to evaluate the consistency and the performance of the proposed control approach. The commonly used European drive cycle ECE-15 is adopted for simulation. The obtained results seem to be very promising. Then, the proposed control approach was experimentally implemented, on a TMS320F240 DSP-based development board, and tested on 1-kW induction motor. Experimental results show that the proposed control scheme is effective in terms of speed and torque performances. Indeed, it allows speed and torque ripple minimization. Moreover, the obtained results show that the proposed sensorless DTC scheme for induction motors is a good candidate for EVs propulsion.**

***Index Terms*—Electric vehicle, Induction motor, sensorless drive, direct torque control, vehicle dynamics.**

I. Introduction

Recently a lot of effort was focused on the development of high performance EV drives. This is mainly to reduce the environmental pollution due to emissions from internal combustion engine (ICE) driven vehicles. EVs are already commercially available; however, they have not yet used the most remarkable advantages of electric motors. Indeed, an electric motor offers very fast response and can be controlled in a much better way; therefore, motion control through precise control of the motors has definite advantages over the ICE driven vehicles. Moreover, adhesion characteristics between tire and road surface are greatly affected by the traction motor control. This means that the stability and safety of EVs can be addressed and then improved by means of motor control.

F. Khoucha* and M.E.H. Benbouzid are with the University of Brest, EA 4325 LBMS, Rue de Kergoat, CS 93837, 29238 Brest Cedex 03, France (e-mail: m.benbouzid@ieee.org). *F. Khoucha is also with the Electrical Engineering Department, Polytechnic Military Academy, 16111 Algiers, Algeria.

K. Marouani and A. Kheloui are with the Electrical Engineering Department, Polytechnic Military Academy, 16111 Algiers, Algeria.

The electric propulsion system is the heart of EVs [1-2]. It consists of the motor drive, transmission device, and wheels. In fact, the motor drive, composed of the electric motor, the power converter, and the electronic controller, is the core of the EV propulsion system. The motor drive is configured to respond to a torque demand set by the driver. The accelerator position provides a torque demand as a fraction of the maximum available torque. Similarly, the first portion of the brake pedal travel is used to derive a regenerative torque demand; the remaining pedal travel brings in a set of standard mechanical brakes.

For EV propulsion, the cage induction motor seems to be the candidate that best fulfils the propulsion major features [3-4]. Induction motor drive control techniques are well documented in literature. The most popular is the so-called vector control technique that is now used for high impact automotive applications (EV and HEV). In this case, the torque control is extended to transient states and allows better dynamic performances [5]. Among these techniques, DTC appears to be very convenient for EV applications [6-11].

The implementation of direct torque control techniques requires precise knowledge of the rotor or stator flux level and position. If a mechanical speed sensor is mounted on the motor shaft, different ways can be used to obtain the flux estimate. But, the current tendency is to eliminate mechanical transducers. Indeed, they are noise sensitive, expensive, bulky, and they tend to reduce the global drive reliability especially in hostile environments that is case with the induction motor within an EV. In this context, several methods have been proposed this last decade for induction motor sensorless speed control [12-15]. Adaptive speed observers seem to be among the most promising methods thanks to their good performance versus computing time ratio. They have the advantage of providing both flux and mechanical speed estimates without problems of open-loop integration [16-17]. Even if some undesirable effects, such as limit cycles, higher noise sensitivity, or delays may occur and deteriorate the system overall performances as raised in [18]. Besides, the adaptive observer has the interesting property of providing a mechanism for on-line tuning of key model parameters such as the stator or rotor resistance and then to compensate for their drift due to motor heating for example [19].

In this paper a sensorless control is proposed to increase the efficiency of a DTC induction motor propelling an EV. The proposed scheme uses an adaptive flux and speed observer that is based on a full order model of the induction motor [20-22] The objective is to test the effectiveness of the

proposed strategy on the whole vehicle and not on the sole induction motor. Simulations were firstly carried out on a test vehicle propelled by a 37-kW induction motor to evaluate the consistency and the performance of the proposed control approach. Then, the proposed control approach was experimentally implemented, on a TMS320F240 DSP-based development board, and tested on a 1-kW induction motor.

II. Vehicle Dynamic Analysis

A. Nomenclature

v = vehicle speed;
α = Grade angle;
P_v = Vehicle driving power;
F_w = Road load;
F_{ro} = Rolling resistance force;
F_{sf} = Stokes or viscous friction force;
F_{ad} = Aerodynamic drag force;
F_{cr} = Climbing and downgrade resistance force;
μ = Tire rolling resistance coefficient ($0.015 < \mu < 0.3$);
m = Vehicle mass;
g = Gravitational acceleration constant;
k_A = Stokes coefficient;
ξ = Air density;
C_w = Aerodynamic drag coefficient ($0.2 < C_w < 0.4$);
A_f = Vehicle frontal area;
v_0 = is the head-wind velocity;
F = Tractive force;
k_m = Rotational inertia coefficient ($1.08 < k_m < 1.1$);
a = Vehicle acceleration;
J = Total inertia (rotor and load);
ω_m = Motor mechanical speed;
T_B = Load torque accounting for friction and windage;
T_L = Load torque;
T_m = Motor torque;
i = Transmission ratio;
η_t = Transmission efficiency;
R = Wheel radius;
J_V = Shaft inertia moment;
J_W = Wheel inertia moment;
λ = Wheel slip.

B. Dynamics Analysis

Based on principles of vehicle mechanics and aerodynamics, one can assess both the driving power and energy necessary to ensure vehicle operation (Fig. 1) [5], [23].

1) Road load and tractive force. The road load consists of

$$F_w = F_{ro} + F_{sf} + F_{ad} + F_{cr} \tag{1}$$

The rolling resistance force F_{ro} is produced by the tire flattening at the roadway contact surface.

$$F_{ro} = \mu mg \cos\alpha \tag{2}$$

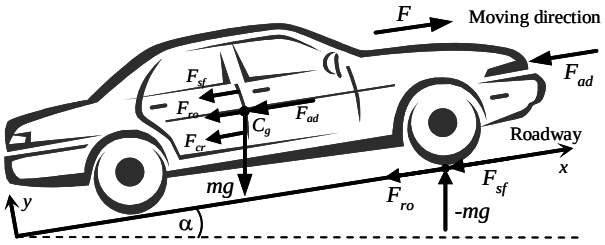

Fig. 1. Elementary forces acting on a vehicle.

μ is nonlinearly dependent on the vehicle speed, tire pressure and type, and road surface characteristic. It increases with vehicle speed and also during vehicle turning maneuvers. The rolling resistance force can be minimized by keeping the tires as much inflated as possible.

$$F_{sf} = k_A v \tag{3}$$

Aerodynamic drag, F_{ad}, is the viscous resistance of air acting upon the vehicle.

$$F_{ad} = \frac{1}{2}\xi C_w A_f (v + v_0)^2 \tag{4}$$

The climbing resistance (F_{cr} with positive operational sign) and the downgrade force (F_{cr} with negative operational sign) is given by

$$F_{cr} = \pm mg \sin\alpha \tag{5}$$

The tractive force in an electric vehicle is supplied by the electric motor to overcome the road load. The equation of motion is given by

$$k_m m \frac{dv}{dt} = F - F_w \tag{6}$$

The net force ($F - F_w$), accelerates the vehicle (or decelerates when F_w exceeds F).

2) Motor ratings and transmission. The power required to drive a vehicle has to compensate the road load F_w.

$$P_v = vF_w \tag{7}$$

The mechanical equation (in the motor referential) used to describe each wheel drive is expressed by

$$J \frac{d\omega_m}{dt} + T_B + T_L = T_m \tag{8}$$

The following equation is derived due to the use of a reduction gear.

$$\begin{cases} \omega_{Wheel} = \dfrac{\omega_m}{i} \\ T_{Wheel} = T_m i \eta_t \end{cases} \tag{9}$$

The load torque in the motor referential is given by.

$$T_L = \frac{T_{LWheel}}{i} = \frac{R}{i} F_\omega \tag{10}$$

The vehicle global inertia moment in the motor referential is given by

$$\begin{cases} J = J_W + J_V \\ J_V = \dfrac{1}{2} m \dfrac{R^2}{i^2}(1-\lambda) \end{cases} \tag{11}$$

If the adhesion coefficient of the road surface is high, then λ is usually low and can be neglected.

III. Adaptive Flux Observer

A. Nomenclature

i_s = Stator current;
φ_r = Rotor flux;
u_s = Stator voltage;
R_s (R_r) = Stator (rotor) resistance;
L_s (L_r) = Stator (rotor) inductance;
M = Mutual inductance;
σ = Total leakage coefficient, $\sigma = 1 - M^2/L_sL_r$;
ω_r = Motor angular velocity;
$\wedge$ = Estimated value;
K = Observer gain matrix.

B. Induction Motor Flux Observer

An induction motor can be described, in the α-β stationary reference frame fixed on stator, by the following state equations.

$$\begin{cases} \dfrac{d}{dt}\begin{bmatrix} i_s \\ \varphi_r \end{bmatrix} = \begin{bmatrix} A_{11} & A_{12} \\ A_{21} & A_{22} \end{bmatrix}\begin{bmatrix} i_s \\ \varphi_r \end{bmatrix} + \begin{bmatrix} B_1 \\ 0 \end{bmatrix} u_s = Ax + Bu \\ i_s = Cx \end{cases} \tag{12}$$

Where $i_s = \begin{bmatrix} i_{s\alpha} & i_{s\beta} \end{bmatrix}^T$, $\varphi_r = \begin{bmatrix} \varphi_{r\alpha} & \varphi_{r\beta} \end{bmatrix}^T$, $u_s = \begin{bmatrix} u_{s\alpha} & u_{s\beta} \end{bmatrix}^T$

and $A_{11} = -\left(\dfrac{1-\sigma}{T_r} + \dfrac{1}{T_s}\right) \Big/ \sigma I$, $A_{12} = M / \sigma L_r L_s T_r I - \omega_r J$

$$A_{21} = 1/\sigma L_r I, \quad A_{22} = -I/T_r + \omega_r J, \quad B_1 = 1/\sigma L_r I$$

$$C = \begin{bmatrix} I & 0 \end{bmatrix}, \quad I = \begin{bmatrix} 1 & 0 \\ 0 & 1 \end{bmatrix}, \quad J = \begin{bmatrix} 0 & -1 \\ 1 & 0 \end{bmatrix}$$

Therefore, a state observer that provides rotor flux estimates is given by

$$\frac{d}{dt}\hat{x} = \hat{A}\hat{x} + Bu + K(\hat{i}_s - i_s) \tag{13}$$

B. Adaptive Flux Observer for Speed Estimation

The induction motor speed in the above observer is not measured and is treated as an unknown parameter. By adding an adaptive scheme for estimating the rotor speed, both states and unknown parameters can be estimated simultaneously. Using Lyapunov stability theory, we can build a mechanism to adapt the mechanical speed from the asymptotic convergence condition of the state variable estimation errors [16], [24].

$$\hat{\omega}_r = K_{I\omega} \int \left[\hat{\varphi}_{r\beta} e_{is\alpha} - \hat{\varphi}_{r\alpha} e_{is\beta} \right] dt \tag{14}$$

Although the adaptive scheme is derived under a constant speed motor consideration, in practice it can change quickly. In order to improve the speed estimation algorithm dynamic behavior, a proportional term can be added [24]. The estimated speed becomes

$$\hat{\omega}_r = K_{I\omega} \int \left[\hat{\varphi}_{r\beta} e_{is\alpha} - \hat{\varphi}_{r\alpha} e_{is\beta} \right] dt + K_{P\omega} \left[\hat{\varphi}_{r\beta} e_{is\alpha} - \hat{\varphi}_{r\alpha} e_{is\beta} \right] \tag{15}$$

IV. Direct Torque Control

A block diagram of the Direct Torque Control scheme is shown by Fig. 2. The control system comprises three basic functions: a two-level hysteresis controller for flux control, a three-level hysteresis controller for torque control, and an optimal switching vector look-up table. The observer estimates the developed torque, stator flux, and shaft speed using measurements of two stator phase currents and the dc-link voltage (V_{dc}). Torque and flux references are compared to their estimated values and control signals are generated using a torque and flux hysteresis control method. The switching vector look-up table (Fig. 3) gives the optimum selection of the switching vectors for all the possible stator flux-linkage space-vector positions. Speed control is achieved using a PI speed controller.

The voltage sensor measures the dc-link voltage that, in conjunction with the knowledge of the switching status of the six controlled power switches of the inverter, is used to compute the stator voltages of the motor using the inverter voltage vector.

$$\begin{cases} V_{s\alpha} = \dfrac{2}{3} V_{dc} \left(S_a - \dfrac{S_b + S_c}{2} \right) \\ V_{s\beta} = \dfrac{1}{\sqrt{3}} V_{dc} \left(S_b - S_c \right) \end{cases} \tag{16}$$

The α-β stator current space vector components are calculated as follows

$$\begin{cases} i_{s\alpha} = i_{Sa} \\ i_{s\beta} = \dfrac{i_{Sa} + 2 i_{Sb}}{\sqrt{3}} \end{cases} \tag{17}$$

The stator flux is a function of the rotor flux that is given by the adaptive flux observer and is calculated by

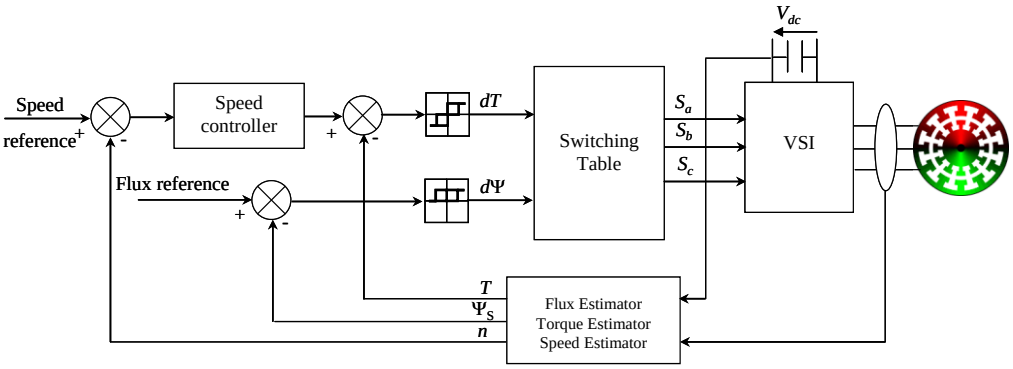

Fig. 2. Typical structure of a sensorless DTC induction motor.

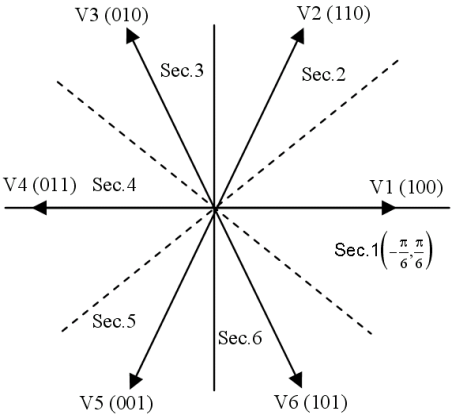

(a) Output voltage vectors.

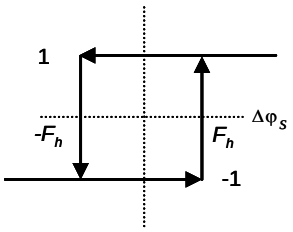

(b) Flux comparator.

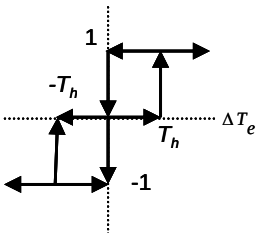

(c) Three-level torque comparator.

		Sector 6 (-90°, -30°)	Sector 5 (-30°, 30°)	Sector 4 (30°, 90°)	Sector 3 (90°, 150°)	Sector 2 (150°, 210)	Sector 1 (210°,270°)
Decrease Flux	Increase Torque	100	110	010	011	001	101
	Decrease Torque	011	001	101	100	110	010
Increase Flux	Increase Torque	110	010	011	001	101	100
	Decrease Torque	001	101	100	110	010	011

(d) Switching table.

Fig. 3. Switching table and comparators for the induction motor DTC.

$$\begin{cases} \varphi_{s\alpha} = \sigma L_s i_{s\alpha} + \dfrac{M}{L_r}\varphi_{r\alpha} \\ \varphi_{s\beta} = \sigma L_s i_{s\beta} + \dfrac{M}{L_r}\varphi_{r\beta} \end{cases} \tag{18}$$

Then the stator flux and the electromagnetic torque are calculated as

$$|\varphi_s| = \sqrt{\varphi_{s\alpha}^2 + \varphi_{s\beta}^2} \tag{19}$$

$$T_e = \frac{3}{2} p \left(\varphi_{s\alpha} i_{s\beta} - \varphi_{s\beta} i_{s\alpha} \right) \tag{20}$$

where p is the pole pair number.

As shown in Fig. 3, a switching table is used for the inverter control such that the torque and flux errors are kept within the specified bands. The torque and flux errors are respectively defined by

$$\begin{cases} \Delta T_e = T_e - \hat{T}_e \\ \Delta \varphi_s = \varphi_s - \hat{\varphi}_s \end{cases} \tag{21}$$

and the inverter switching states are determined by the torque and flux errors according to the determined sector. When the torque is equal or close to its reference value, the three VSI voltage vectors should be arranged in a symmetrical order.

V. Simulations Results

Numerical simulations were carried out on an EV propelled by a 37-kW induction motor drive whose ratings are summarized in the appendix. The electrical vehicle mechanical and aerodynamic characteristics are also given in the appendix. The objectives of the simulations which were carried out were to assess the efficiency and dynamic performances of the proposed sensorless DTC strategy. Figure 4 gives the global configuration of the sensorless DTC scheme and also shows how the EV dynamics will be taken into account. The test cycle is the urban ECE-15 cycle [25]. A driving cycle is a series of data points representing the vehicle speed versus time. It is characterized by low vehicle speed (maximum 50 km/h) and is useful for testing electrical vehicles performance in urban areas.

For sensorless purposes, an estimator scheme for the rotor speed, the torque and the flux is proposed on a fourth-order electrical model basis. The sensorless DTC strategy performances are first illustrated by Figs. 5 and 6 that show, respectively, the speed and the developed torque with changes of the acceleration pedal position and a varied road profile. It should be noticed that speed and torque variations are as large as are the variations of the accelerator pedal and the road profile. It is obvious that the proposed strategy operates satisfactorily.

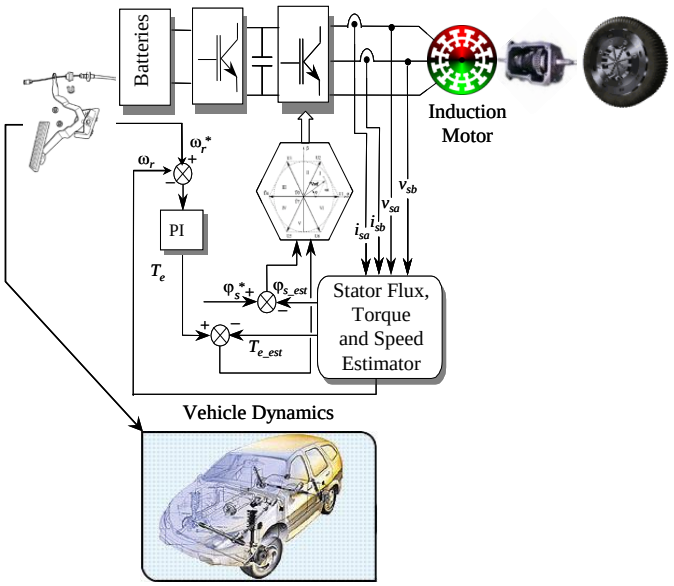

(a)

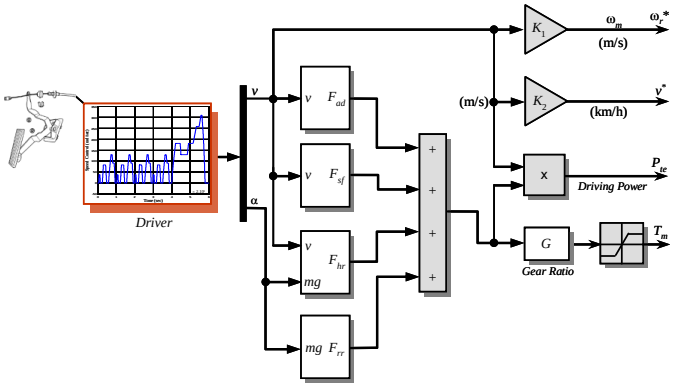

(b) EV dynamics.

Fig. 4. Scheme for the EV sensorless DTC simulation.

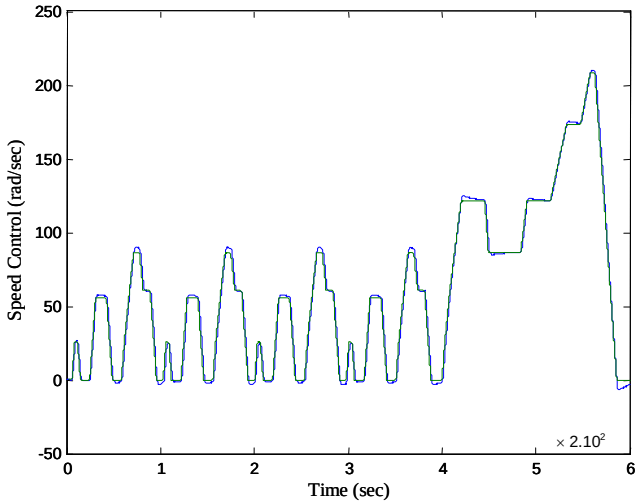

Fig. 5. Estimated and measured vehicle speed.

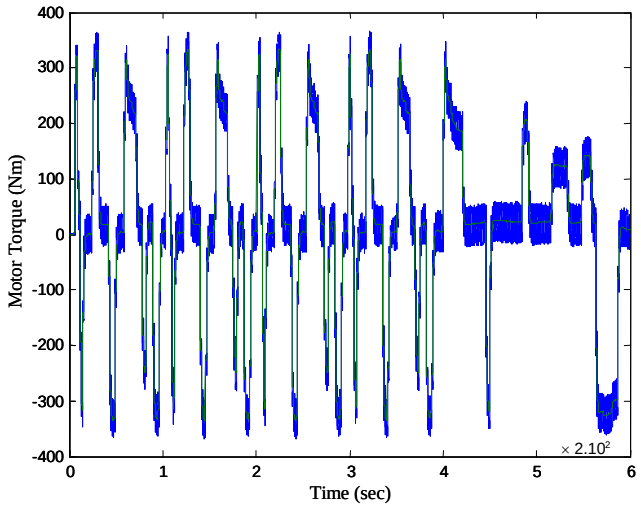

Fig. 6. Developed and estimated motor torque.

VI. Experimental Results

A. The Experimental Setup

The main components of the experimental setup are (Fig. 7): a DSP system (single fixed-point TMS320F240 DSP-based development board), an optical encoder attached to the motor shaft only to allow comparison between estimated and measured speed, and current sensors. The DSP system is interfaced to a standard PC. The continuous-time algorithm is discredited with a sampling period of 100 µsec. At each sampling instant, the DSP receives stator current and voltage measurements and then runs the estimation algorithm and the DTC scheme.

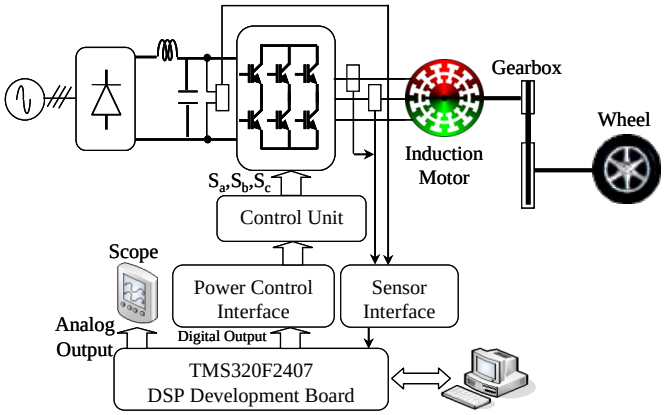

Fig. 7. The experimental setup.

B. The Experiments

Experimental tests have been carried out to test the estimation algorithm. For that purpose, a 1-kW induction motor drive, whose ratings are summarized in the appendix, has been used. In this case the EV dynamics is not taken into account.

The estimation algorithm was tested in various speed regions and various conditions. As shown in Fig. 8, the estimator was seen to work well under various circumstances. Hence the proposed approach (DTC associated to a full order observer estimator) allows the torque, the rotor speed, and the current ripple to be reduced that is of great importance for an EV application, in terms of efficiency improvement (current ripple minimization) and dynamic performances improvement (speed and torque ripple minimization).

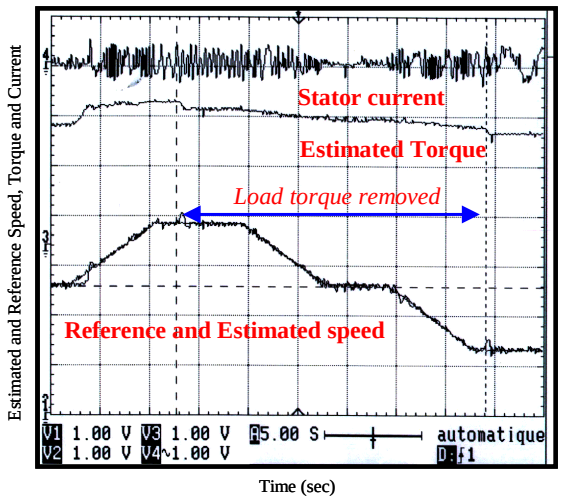

(a) From low to high speed operation.

VII. Conclusion

In this paper a sensorless control was proposed to increase the efficiency of a DTC induction motor propelling an EV. The proposed scheme uses an adaptive flux and speed observer that is based on a full order model of the induction motor. It was successfully simulated on a 37-kW induction motor drive taking into account the vehicle dynamics. In this case, the commonly used European drive cycle ECE-15 was adopted. The estimation was then experimentally tested on a 1-kW induction motor drive. Experimental results show that the sensorless scheme is effective in terms of speed and torque performance. Indeed, it is capable of working from very low to high speed and exhibits very good dynamics.

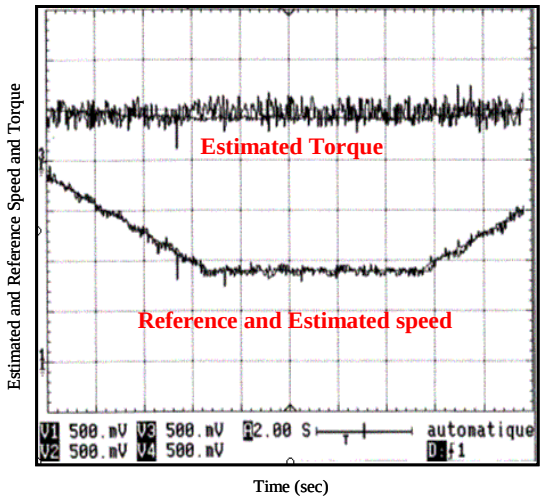

(b) Low speed operation at rated load.

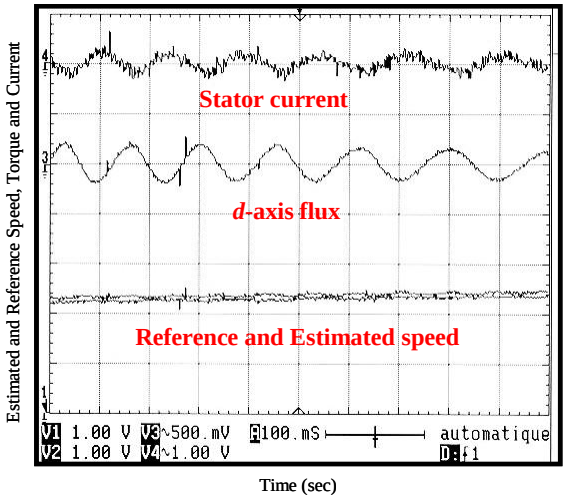

(c) Zoom during low speed operation.

Fig. 8. Experimental results.

Moreover, the proposed approach (DTC associated to a full order observer estimator) allows the torque, the rotor speed, and the current ripple to be reduced.

The obtained results show that the proposed sensorless DTC induction motor drive scheme should be considered as a good candidate for EV propulsion.

APPENDIX

RATED DATA OF THE SIMULATED INDUCTION MOTOR

37 kW, 50 Hz, 400/230 V, 64/111 A, 24.17 Nm, 2960 rpm
R_s = 85.1 mΩ, R_r = 65.8 mΩ
L_s = 31.4 mH, L_r = 29.1 mH, L_m = 29.1 mH
J = 0.23 kg.m²

RATED DATA OF THE TESTED INDUCTION MOTOR

1 kW, 50 Hz, 400/230 V, 3.4/5.9 A, 7 Nm, 2890 rpm
R_s = 4.67 Ω, R_r = 8 Ω, L_s = L_r = 0.347 H, M = 0.366 H
J = 0.06 kg.m², β = 0.042 Nm.sec

EV MECHANICAL AND AERODYNAMIC PARAMETERS

m = 1540 kg (two 70 kg passengers), A = 1.8 m^2, r = 0.3 m
μ_{rr1} = 0.0055, μ_{rr2}=0.056, C_{ad} = 0.19, G = 104, η_g = 0.95
T = 57.2 Nm (stall torque), v_0 = 4.155 m/sec
g = 9.81 m/sec^2, ρ = 0.23 kg/m^3

REFERENCES

[1] C.C. Chan et *al.*, "Electric vehicles charge forward," *IEEE Power and Energy Magazine*, vol. 2, n°6, pp. November-December 2004.

[2] C.C. Chan, "The state of the art of electric and hybrid vehicles," *Proceedings of the IEEE*, vol. 90, n°2, pp. 247-275, February 2002.

[3] M. Zeraoulia et *al.*, "Electric motor drive selection issues for HEV propulsion systems: A comparative study," *IEEE Trans. Vehicular Technology*, vol. 55, n°6, pp. 1756-1764, November 2006.

[4] D. Diallo et *al.*, "A fault-tolerant control architecture for induction motor drives in automotive applications," *IEEE Trans. Vehicular Technology*, vol. 53, n°6, pp. 1847-1855, November 2004.

[5] S.N. Vukosavic et *al.*, "A method for transient torque response improvement in optimum efficiency induction motor drives," *IEEE Trans. Energy Conversion*, vol. 18, n°4, pp. 484-493, December 2003.

[6] A. Haddoun et *al.*, "A loss-minimization DTC scheme for EV induction motors," *IEEE Trans. Vehicular Technology*, vol. 56, n°1, pp. 81-88, January 2007.

[7] M. Bertoluzzo et *al.*, "Direct torque control of an induction motor using a single current sensor," *IEEE Trans. Industrial Electronics*, vol. 53, n°3, pp 778-784, June 2006.

[8] G.S. Buja et *al.*, "Direct torque control of PWM inverter-fed ac motors—A survey," *IEEE Trans. Industrial Electronics*, vol. 51, n°4, pp 744-757, August 2004.

[9] D.O. Neacsu et *al.*, "Comparative analysis of torque-controlled IM drives with applications in electric and hybrid vehicles vehicle," *IEEE Trans. Power Electronics*, vol. 16, n°2, pp. 240-247, March 2001.

[10] J. Faiz et *al*, "Direct torque control of induction motor for electric propulsion systems", *Electric Power Systems Research*, vol. 51, pp. 95-101, 1999.

[11] N. Mutoh et *al*, "A torque controller suitable for electric vehicles," *IEEE Trans. Industrial Electronics*, vol. 44, n°1, pp. 54-63, February 1997.

[12] B.K. Bose et *al.*, "A start-up method for a speed sensorless stator-flux-oriented vector-controlled induction motor drive," *IEEE Trans. Industrial Electronics*, vol. 44, n°4, pp 587-590, August 1997.

[13] J. Faiz et *al.*, "Sensorless direct torque control of induction motors used in electric vehicle," *IEEE Trans. Energy Conversion*, vol. 18, n°1, pp. 1-10, March 2003.

[14] C. Lascu et *al.*, "A sensorless hybrid DTC drive for high-volume low-cost applications," *IEEE Trans. Industrial Electronics*, vol. 51, n°5, pp 1048-1055, October 2004.

[15] K. Jezernik, "Speed sensorless torque control of induction motor for EV's", *in Proceedings of IEEE IWAMC'02*, pp. 236-241, Maribor (Slovenia), 2002.

[16] L. Harnefors, "Globally Stable Speed-Adaptive Observers for Sensorless Induction Motor Drives," *IEEE Trans. Industrial Electronics*, vol. 54, n°2, pp 1243-1245, April 2007.

[17] M. Depenbrock et *al.*, "Model-based speed identification for induction Machines in the whole operating range," *IEEE Trans. Industrial Electronics*, vol. 53, n°1, pp 31-40, February 2006.

[18] C. Lascu et *al.*, "Sliding-mode observer and improved integrator with DC-offset compensation for flux estimation in sensorless-controlled

induction motors," *IEEE Trans. Industrial Electronics*, vol. 53, n°3, pp 785-794, June 2006.
[19] J. Faiz et *al.*, "Different techniques for real time estimation of an induction motor rotor resistance in sensorless direct torque control for electric vehicle," *IEEE Trans. Energy Conversion*, vol. 16, n°1, pp. 104-109, March 2001.
[20] J. Salomaki et *al.*, "Sensorless control of induction motor drives equipped with inverter output filter," *IEEE Trans. Industrial Electronics*, vol. 53, n°4, pp 1188-1197, August 2006.
[21] M. Hasegawa, "Robust-adaptive-observer design based on γ-positive real problem for sensorless induction-motor drives," *IEEE Trans. Industrial Electronics*, vol. 53, n°1, pp 76-85, February 2006.
[22] S. Suwankawin et *al.*, "Design strategy of an adaptive full-order observer for speed-sensorless induction-motor drives-tracking performance and stabilization," *IEEE Trans. Industrial Electronics*, vol. 53, n°1, pp 96-119, February 2006.
[23] I. Husain et *al.*, "Design, modeling and simulation of an electric vehicle system," *SAE Technical Paper Series*, Paper # 1999-01-1149.
[24] M. Hinkkanen, "Analysis and design of full-order flux observers for sensorless induction motors," *IEEE Trans. Industrial Electronics*, vol. 51, n°5, pp. 1033-1040, October 2004.
[25] M. André et *al.*, "Driving cycles for emissions measurements under European Conditions," *SAE Paper* # 950926, pp. 193-205, 1995.

Farid Khoucha was born in Khenchela, Algeria, in 1974. He received the B.Sc. and the M.Sc. degrees in Electrical Engineering, from the Polytechnic Military Academy, Algiers, Algeria, in 1998 and 2003 respectively. In 2000, he joined the Electrical Engineering Department of the Polytechnic Military Academy, Algiers, Algeria as a Teaching Assistant.

He is currently pursuing Ph.D. studies on electric and hybrid vehicle control and power management.

Khoudir Marouani was born in Constantine, Algeria, in 1972. He received the B.Sc. and the M.Sc. degrees in Electrical Engineering, from the Polytechnic Military Academy, Algiers, Algeria, in 1996 and 2000 respectively. In 2000, he joined the Electrical Engineering Department of the Polytechnic Military Academy, Algiers, Algeria as a Teaching Assistant.

He is currently pursuing Ph.D. studies. His main research interests include power electronics, electrical drives and active power filters.

Abdelaziz Kheloui received the M.Sc. degree in Electrical Engineering from the Ecole Nationale d'Ingénieurs et Techniciens of Algeria (ENITA), Algiers, Algeria in 1990 and the Ph.D. degree also in Electrical Engineering from the National Polytechnic Institute of Lorraine, Nancy, France in 1994. Since 1994 he has been an Assistant than an Associate Professor at the Electrical Engineering Department of the Polytechnic Military Academy, Algiers, Algeria.

His current research interests are control of electrical drives and power electronics.

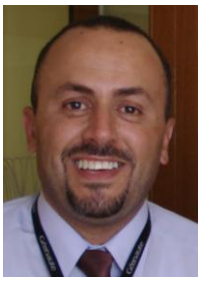

Mohamed El Hachemi Benbouzid was born in Batna, Algeria, in 1968. He received the B.Sc. degree in electrical engineering from the University of Batna, Batna, Algeria, in 1990, the M.Sc. and Ph.D. degrees in electrical and computer engineering from the National Polytechnic Institute of Grenoble, Grenoble, France, in 1991 and 1994, respectively, and the Habilitation à Diriger des Recherches degree from the University of Picardie "Jules Verne," Amiens, France, in 2000.

After receiving the Ph.D. degree, he joined the Professional Institute of Amiens, University of Picardie "Jules Verne," where he was an Associate Professor of electrical and computer engineering. In September 2004, he joined the University Institute of Technology (IUT) of Brest, University of Western Brittany, Brest, France, as a Professor of electrical engineering. His main research interests and experience include analysis, design, and control of electric machines, variable-speed drives for traction and propulsion applications, and fault diagnosis of electric machines.

Prof. Benbouzid is a Senior Member of the IEEE Power Engineering, Industrial Electronics, Industry Applications, Power Electronics, and Vehicular Technology Societies. He is an Associate Editor of the IEEE TRANSACTIONS ON ENERGY CONVERSION, the IEEE TRANSACTIONS ON INDUSTRIAL ELECTRONICS, the IEEE TRANSACTIONS ON VEHICULAR TECHNOLOGY, and the IEEE/ASME TRANSACTIONS ON MECHATRONICS.